



City Research Online

## City, University of London Institutional Repository

---

**Citation:** Cao, X., Ren, Y., Qian, K., Fu, F. & Zhang, W. (2022). Size effect on flexural behavior of ultra-high-performance concrete beams with different reinforcement. *Structures*, 41, pp. 969-981. doi: 10.1016/j.istruc.2022.05.062

This is the accepted version of the paper.

This version of the publication may differ from the final published version.

---

**Permanent repository link:** <https://openaccess.city.ac.uk/id/eprint/28204/>

**Link to published version:** <https://doi.org/10.1016/j.istruc.2022.05.062>

**Copyright:** City Research Online aims to make research outputs of City, University of London available to a wider audience. Copyright and Moral Rights remain with the author(s) and/or copyright holders. URLs from City Research Online may be freely distributed and linked to.

**Reuse:** Copies of full items can be used for personal research or study, educational, or not-for-profit purposes without prior permission or charge. Provided that the authors, title and full bibliographic details are credited, a hyperlink and/or URL is given for the original metadata page and the content is not changed in any way.

---

---

---

City Research Online:

<http://openaccess.city.ac.uk/>

[publications@city.ac.uk](mailto:publications@city.ac.uk)

---

# Size effect on flexural behavior of ultra-high-performance concrete beams with different reinforcement

Xia Cao<sup>a,b</sup>, Yi-Cheng Ren<sup>a,b</sup>, Kai Qian<sup>a,b</sup>, Feng Fu<sup>c 1</sup>, Xiao-Fang Deng<sup>a,b 2</sup>, Wei-Jia Zhang<sup>a,b</sup>  
<sup>a</sup> Guang Xi Key Laboratory of New Energy and Building Energy Saving, Guilin 541004, China  
<sup>b</sup> College of Civil and Architecture Engineering, Guilin University of Technology, Guilin 541004, China  
<sup>c</sup> School of Mathematics, Computer Science and Engineering, City, University of London, EC1V0HB, UK

## Abstract

In this paper, in order to investigate the size effect on the flexural behavior of ultra-high-performance concrete (UHPC) beams, two groups UHPC beams with sizes of, 150mm×250mm×2300mm (small) and 300mm×500mm×4600mm (large), were tested through four-point bending test. Each group consists of four UHPC beams with different rebar type and reinforcement ratio. The experimental results showed that the flexural strength, normalized deflection, and fracture toughness of HRB400 steel reinforced UHPC beams was not affected by size effect. The normalized deflection at ultimate bearing capacity of GFRP reinforced UHPC beams is affected by size effect, but no size effect was shown for whole deflection process. The flexural strength and fracture toughness of GFRP reinforced UHPC beams changed from having size effect to no size effect with the increase of reinforcement ratio. Furthermore, the maximum crack width, number of cracks and average crack spacing of both UHPC beams were sensitive to the size of specimen, while no significant size effect was shown for ductility of both UHPC beams.

---

<sup>1</sup> Corresponding author email: [feng.fu.1@city.ac.uk](mailto:feng.fu.1@city.ac.uk) (Feng Fu)

<sup>2</sup> Corresponding author email: [dengxiaofang@glut.edu.cn](mailto:dengxiaofang@glut.edu.cn) (Xiao-Fang Deng)

**Key words:** ultra-high-performance concrete, four-point bending beams, flexural behavior, size effect

## **1. Introduction**

With the development of construction technology, the size of steel reinforced concrete structural members become larger. However, the current design method of steel reinforced concrete beams is based on the test results of small size members, which is different from the actual behavior of large structural members in engineering. Therefore, when designing large size structural members, it is necessary to consider the influence of size effect on their performance.

There are three major approaches to explain the size effect of the concrete or concrete members: Weibull's theory[1], Bažant's theory[2] and fractal theory of fracture [3]. Weibull's theory [1] states that the size effect is mainly caused by the random distribution of material strength. The probability of encountering a low strength material element increases with the increase of structure size due to the randomness of concrete strength. Bažant's theory [2] suggests that the size effect is caused by the steady growth of macroscopic crack propagation with load, stress redistribution and release of stored strain energy. The fractal theory of fracture [3] considered that the size effect is caused by the difference of fractal characteristics during fracture propagation in quasi-brittle materials.

Many experts and scholars have conducted in-depth studies on the size effects of concrete members[4]-[8]. Lepech et al.[9] investigated the size effect on the flexural behavior of engineered cement composites (ECCs). The results indicated that the size

effect on the flexural strength of ECC members was negligible when compared to reinforced concrete specimens. Kim et al. [10] also carried out bending tests for fiber-reinforced cementitious composites (FRCCs) with three different sizes. The results illustrated that the flexural strength and normalized deformation of FRCC increase with the decrease of size, and the flexural behavior of FRCC has obvious size effect. Alca et al.[11] studied the influence of size effects on the flexural strength of high-strength concrete beams. They found that there was no significant size effect on the flexural strength of high strength concrete beams. However, Appa et al[12]concluded that there are obvious size effects on both flexural capacity and ductility of steel reinforced concrete beams.

Compared to regular, fiber-reinforced concrete, etc, Ultra-high-performance concrete (UHPC) is characterized by high compressive strength, high toughness, and high durability [13-15]. Therefore, UHPC is gradually used in engineering field such as bridge structure, building structures and repair work etc. In recent years, some scholars have studied the influence of size effect on the flexural performance of UHPC [16-21]. Mahmud et al. [16] and Wille et al. [17] conducted three-point and four-point bending tests on UHPC beams. The results showed that the size effect had no effect on the flexural strength of UHPC beams, owing to the high ductility of UHPC. Nguyen et al [18] conducted four-point bending tests on UHP-HFRC with three sizes. They found that the flexural strength, normalized strength, and normalized energy absorption capacity of UHP-HFRC exhibited size effects. This is consistent with the findings from Chandrangsu et al.[21], but not with Mahmud et al[16] and Wille et al [17]. Yoo et al.

[19] studied the influence of different types of steel fibers on the size effect of UHPC beams. The results illustrated that compared with the steel fiber with small aspect ratio, the steel fiber with large aspect ratio could effectively reduce the size effect of UHPC beam, and the flexural strength of the UHPC beam with 2% volume content of steel fiber was not significantly affected by the size effect. Reineck et al[20] investigated the influence of specimen size on the tensile and flexural strength of UHPFRC. They found that the ratio of the width to length of the specimen section was one of the key parameters affecting the tensile and bending strength of UHPFRC. Overall, there is little research on the size effect of the UHPC beams, especially in the aspects of reinforcement ratio and rebar type. The influence of size effect on the flexural performance of UHPC beams is still not clear and the conclusions are not sufficient. The size effect of UHPC beam needs further study.

The study aimed to investigate the size effect on the flexural behavior of the UHPC beam that the research variables were reinforcement type and reinforcement ratio. Two reinforcement ratio 0.68% and 1.17%, and two types of rebars GFRP and HRB400 steel reinforcement were used in the study. Two different sizes of UHPC beams, 150mm×250mm×2300mm (small) and 300mm×500mm×4600mm (large) selected. Four-point bending tests were performed to investigate the influence of size effect on flexural capacity, normalized deflection, cracking behavior, fracture toughness and ductility, etc.

## **2. Test set up**

### **2.1 Specimen characteristics**

The mix design and mechanical properties of the UHPC matrix are summarized in Table 1 and Table 2, respectively. The diameter and length of steel fibers were 0.22mm and 13mm, respectively, and their properties are provided in Table 3. According to the geometric similarity principle, rebar type and reinforcement ratio, a total of eight UHPC beams were prepared in the experimental program under two different sizes: 150mm × 250mm × 2300mm (small) and 300mm × 500mm × 4600mm (large). The tensile reinforcements were GFRP rebars and HRB400 steel reinforcements, respectively. The reinforcement ratio was 0.68% and 1.17%, respectively, and the stirrup adopted HRB400 steel reinforcements. The specimens were grouped into two series—a beam series reinforced with GFRP rebars (G-X-X) and a beam series reinforced with HRB400 steel reinforcements (S-X-X). The letters G, S, 0.68/1.17, and 250/500 indicate the GFRP rebar, HRB400 steel rebar, reinforcement ratio, and the specimen height, respectively. For example, the specimen G-0.68-250 is composed of the GFRP bars reinforced UHPC beam with 0.68% reinforcement ratio and specimen height of 250mm. The geometrical shape and reinforcement of test beams are shown in Figure 1 and Table 4. The properties of used rebars are summarized in Table 5.

### **2.2 Materials and specimen preparation**

Silica sand, as the only aggregate in UHPC, contained three particle sizes, namely fine (0.16-0.315mm), medium (0.315-0.63mm), and coarse (0.63-1.25mm). The 2% dosage (2 vol.%) of straight steel fibers and 2% of polycarboxylate superplasticizer was

incorporated. Further, Portland cement (PO42.5) and silica fume (silica flour with 98% SiO<sub>2</sub> at 0.3 μm average diameter) were used as the cementitious materials.

To fabricate flowable UHPC, three different grades of silica sand was first premixed for 2 min. Secondly, the steel fibers were dispersed into the mixture and mixed for 2 min. Thirdly, cement and silica fume were added and mixed for another 10 min. Lastly, water premixed with superplasticizer was poured into the dry mixture and mixed for another 6 min, consistently. Ultra-high-performance concrete with good compatibility and workability could be obtained.

Because UHPC had adequate workability and showed self-consolidating characteristics, the structural elements made of this material are generally fabricated by casting the concrete at a certain point and allowing it to flow[22]-[25]. Therefore, all test UHPC beams were fabricated in the same way that UHPC was poured at the end and allowed to self-flow. The specimens were covered with sponges and allowed to harden at room temperature for one day. All the specimens were then taken out of the moulds and were cured at room temperature for 28 days.

As the behavior such as bond behavior of GFRP rebar [26,27] and steel reinforcement is different, so in this research both GFRP rebars and HRB400 steel reinforcement are used

### **2.3 Test setup and Test procedure**

The test rigs are shown in Figure 2. The test was implemented by load and displacement through hybrid control method[28-33]. The test used load control before cracking. Before the load reached 90% of the estimated crack load of the test beam, the

increasing value of each increment was 5% of the estimated ultimate load. The loading value of each level did not exceed 5kN when it was close to the cracking load. When the test beam cracked, the test used displacement control and the speed was 1 mm/min until failure. The load of each increment was maintained for 5 min.

## **2.4 Test content**

To pinpoint the cracking and capture the growth of cracks in the test process, a thin layer of white paint was alternatively applied before testing. The detailed testing content are illustrated as following: (i) Strain gages were attached at the longitudinal reinforcements (Figure1(a、 b)) to measure the strains in the reinforcements. (ii) The deflection of beam span, loading point and support position was measured using LVDTs (Figure 2); (iii) The cracking load and ultimate load, test phenomenon and failure pattern of the test beam are recorded, simultaneously.

## **3. Experimental results and discussion**

### **3.1 Failure modes**

Figure 3 shows the cracking behavior of UHPC beam under four-point bending test. As shown in Figure 3, the UHPC beams under four-point bending can be divided into two zones: zone 1 and zone 2. Zone 1 was pure bending zone. The cracks generated in zone 1 were uniformly distributed. Zone 2 included the two-thirds of the span (one-third each at either side of zone 1) where the cracking behavior was influenced by shear as well as moment [18]. Consequently, the cracks in zone 2 were non-uniform and gradually increased from the support to zone 1. Under four-point bending, multiple closely spaced cracks were developed in zone 1, while relatively few sparsely spaced

cracks developed in zone 2. Figure 4 shows the cracks of the flexural UHPC beams during the test. The cracks within zone 1 were perpendicular to the neutral axis of the UHPC beams while the few cracks within zone 2 were usually inclined due to the shear effect [18].

Figure 5 shows the crack pattern and failure modes. The tensile failure was observed in GFRP rebars reinforced UHPC beams (G-0.68/1.17-250/500), i.e., the tensile GFRP rebars were pulled or broken. However, the UHPC at the edge of the compression zone had not reached the ultimate pressure strain and was not crushed (Figure 5(b)). HRB400 steel rebars reinforced UHPC beams (S-0.68/1.17-250/500) were the balanced-reinforced beam failure showing the tensile reinforcement yielded and the concrete in the compression zone peeled off (Figure 5(c)). Although the beam geometry, boundary and loading conditions are all symmetric, the damage cracks of the test beams were tortuous and deviated away from the beam central lines. This should be attributed to the random distribution and orientation of steel fibres[17],34[34], which made the crack-tip stress fields complicated and the local tensile strength and fracture toughness highly heterogeneous[16].

The failure modes of the UHPC beams with GFRP rebars and HRB400 steel rebars were different at ultimate bearing capacity. The damage crack width of GFRP rebars reinforced UHPC beams increased suddenly, when the UHPC beam reaches the ultimate bearing capacity. The tensile GFRP rebars were pulled and the beams were brittle failure. However, the UHPC beams with HRB400 steel rebars continued to carry higher load. The damage crack width of HRB400 steel rebars reinforced UHPC beams

increased slowly, and the beams performed ductile failure.

### **3.2 Results summary**

Table 6 summarizes the test result of ultimate moment and ultimate load. The maximum crack width, number of cracks and average crack spacing of zone 1 of the UHPC beams are shown in Table 7. Figure 6 shows the load and mid-span deflection curves and strains measured at the center of the longitudinal GFRP and steel rebars are shown in Figure 7. As shown in Table 6, the ultimate bearing capacity of GFRP bars reinforced UHPC beams and HRB400 steel reinforced UHPC beams was large when a higher GFRP/steel reinforcement ratio and specimen size were used.

### **3.3 Relationship between the load and strain in rebars**

Strains measured at the center of the longitudinal GFRP and steel rebars are shown in Figure 7. Before cracking, the strain of GFRP rebars and HRB400 steel reinforcement drove the nearly linear increase. After cracking, the stress was transferred from concrete to GFRP bars and HRB400 steel reinforcements. Due to the low elastic modulus of GFRP bars, the strain of GFRP rebars increased faster than that of HRB400 steel reinforcements. The strain change law of GFRP bars was basically the same as HRB400 steel reinforcements. With the increase of reinforcement ratio, lower strains were observed for the UHPC beams with GFRP rebars and HRB400 steel reinforcements at identical load levels. The strain of GFRP rebars was greater than that of HRB400 steel reinforcements at identical load levels and ultimate bearing capacity.

### **3.4 Load versus deflection response**

Figure 6 shows the load and mid-span deflection curves for test UHPC beams, and

the deflection at ultimate bearing capacity is illustrated in Table 8. The load and deflection curves of GFRP bars reinforced UHPC beams with different sizes were bilinear, while the load and deflection curves of HRB400 steel reinforced UHPC beams had yielding stage. Considering the additional influence that caused by reinforcement ratio, the deflection of GFRP bars reinforced UHPC beams and HRB400 steel reinforced UHPC beams were increasing accordingly. With the increase of reinforcement ratio, lower deflection was observed for the UHPC beams with GFRP rebars and HRB400 steel reinforcements at identical load levels. The deflection at ultimate bearing capacity of UHPC beams with GFRP bars and HRB400 steel reinforcements increased with the increase of specimen size. GFRP bars reinforced UHPC beams had higher deflection at ultimate bearing capacity than that of HRB400 steel reinforced UHPC beams (Table 8).

### **3.5 Ductility**

Since GFRP rebar shows no any yielding behavior and UHPC has higher ductility, conventional definition of ductility index is inappropriate for the evaluation of structural ductility of UHPC beams with GFRP bars and steel bars. Therefore, the energy-based approach was used to calculate ductility, as shown in Eq. (1) [35]. Figure 8(a) illustrates the schematic diagram of the load-deflection curve of FRP-reinforced concrete beams showing the calculated energies as proposed by Naaman and Jeong [35], and Figure 8(b) illustrates load-deflection curve of steel-reinforced concrete beams as proposed by Jo BW et al [36]. As shown in the Figure 8, the un-loading slope was determined using the initial slope and its load ( $S_1$  and  $P_1$ , respectively), and the secant

slope and its load ( $S_2$  and  $P_2$ , respectively). As the behavior of the GFRP bars reinforced UHPC beams were almost bilinear, the  $P_2$  was taken as  $P_u$  in Figure 8(a) [37]. Due to the existence of yield stage in HRB400 steel reinforced UHPC beams, the  $P_1$  was taken as  $P_u$  in Figure 8(b).

$$\mu_e = \frac{1}{2} \left( \frac{E_{tot}}{E_{el}} + 1 \right) \quad (1)$$

$$S = \frac{P_1 S_1 + (P_2 - P_1) S_2}{P_2} \quad (2)$$

Where  $\mu_e$  is the ductility index,  $E_{tot}$  is the total energy, which is the area under load-deflection curve up to the ultimate load =  $A_1 + A_2$  in Figure 8, and  $E_{el}$  is the elastic stored energy, a portion of the total energy =  $A_1$  in Figure 8.

The ductility calculated by the energy-based approach is shown in Table 8. The ductility index of GFRP bars reinforced UHPC beams was 1.176~1.222, while the ductility index of HRB400 steel reinforced UHPC beams was 1.189~1.768. The ductility of UHPC beams with GFRP bars and HRB400 steel bars was low when a higher GFRP or HRB400 steel reinforcement ratio was used. The GFRP bars reinforced UHPC beams produced a low ductility than HRB400 steel reinforced UHPC beams. This was because GFRP rebars had no yielding characteristics, while HRB400 steel reinforcements had yielding characteristics.

## 4. Size effect on flexural behavior of UHPC beams

### 4.1 Size effect on equivalent bending stress

The ultimate bearing capacity of the test beams were expressed by the equivalent bending stress that was calculated from the equation suggested in Wille et al [17] as follows:

$$\sigma_f = \frac{M}{S} = \frac{6 \times M}{b \times h^2} = \frac{PL}{b \times h^2} \quad (3)$$

Where  $M$  is the applied moment,  $P$  is the applied load,  $b$ ,  $h$  are the width and height of the specimen, respectively.

The beam sizes on the variation of the equivalent bending stress were calculated from the test results are illustrated in Figure 9, while the calculation results are shown in Table 6. The ultimate bearing capacity of GFRP bars reinforced UHPC beams with low reinforcement ratio (G-0.68, reinforcement ratio 0.68%) had a certain size effect, i.e., as the beam size increased from 250 mm to 500 mm, the equivalent bending stress at the ultimate bearing capacity decreased. The beam size on the equivalent bending stress for ultimate bearing capacity of GFRP bars reinforced UHPC beams with high reinforcement ratio (G-1.17, reinforcement ratio 1.17%) and all HRB400 steel reinforced UHPC beams had no size effect (Figure 9). This implied that the ultimate bearing capacity of GFRP bars reinforced UHPC beams was affected by size effect due to the brittle property of GFRP bars, but the flexural strength of GFRP reinforced UHPC beams changed from having size effect to no size effect with the increase of the ratio of GFRP bars. In contrast, the ultimate bearing capacity of all HRB400 steel reinforced UHPC beams had no size effect due to the yield characteristics of HRB400 steel rebars.

#### **4.2 Size effect on cracking behavior**

Figure 10 and Table 7 show the maximum crack width, number of cracks and average crack spacing of zone 1 of the UHPC beams, and the crack behavior of the UHPC beams is shown in Figure 5. The number of cracks developed in zone 1 of the UHPC beams was approximately 56%~72% of the total number of cracks counted in

both zone 1 and 2. The average crack spacing decreased with the increase of cracks, which was related to the bending strain capacity of UHPC beams, because the crack spacing in tension was strongly influenced by the tensile strain at the post cracking strength of the UHPC beams: the increase in tensile strain capacity was accompanied by an increase of cracks and a reduction of average crack spacing within the zone 1 of the UHPC beams [18,38]. The average crack spacing of GFRP bars reinforced UHPC beams was more sensitive to specimen size, as shown in Figure 10(c) and Table 7, than that of HRB400 steel reinforced UHPC beams. The average crack spacing for small and large GFRP bars reinforced UHPC beams was 31.58mm, 63.16mm (reinforcement ratio 0.68%), 30.00mm, 57.14mm (reinforcement ratio 1.17%), respectively. The average crack spacing for small and large HRB400 steel reinforced UHPC beams was 25.00mm, 38.71mm (reinforcement ratio 0.68%), 24.00mm, 46.15mm (reinforcement ratio 1.17%), respectively. As shown in Table 7 and Figure 10(a), the different size of GFRP bars reinforced UHPC beams produced a higher maximum crack width than HRB400 steel reinforced UHPC beams when they had identical reinforcement ratios. In contrast to HRB400 steel bars and UHPC, GFRP bars and UHPC were inferior in bonding performance and crack retardation development. Therefore, the maximum crack width of GFRP bars reinforced UHPC beams was more sensitive to specimen size.

Compared with HRB400 steel reinforced UHPC beams, GFRP bars reinforced UHPC beams produced fewer cracks, while the average crack spacing in zone 1 (Figure 3) was larger. Large UHPC beams produced more cracks than small UHPC beams (Figure 10(b)), but the maximum crack width and average crack spacing became larger

with the increase of size (Figure 10(a, c)). This implies that the maximum crack width, number of cracks and average crack spacing of UHPC beams was sensitive to specimen size, and it was not affected by the rebar type and reinforcement ratio.

### 4.3 Size effect on fracture toughness parameter

The fracture toughness ( $K_{IC}$ ) may be taken as the value of stress intensity factor created at the tip of the critical fracture process zone by ultimate load. The fracture toughness of UHPC beams was calculated from the equation suggested in Li and Maalej [39] as follows:

$$K_{IC} = \sigma \sqrt{\pi a} F_1(a/h) \quad (4)$$

$$F_1(a/h) = 1.122 - 1.4 \left(\frac{a}{h}\right) + 7.33 \left(\frac{a}{h}\right)^2 - 13.08 \left(\frac{a}{h}\right)^3 + 14.0 \left(\frac{a}{h}\right)^4 \quad (5)$$

Where  $\sigma = \sigma_{fl}$ , as shown in equation (3),  $a$  is critical crack extension length.

The variations of fracture toughness are plotted with respect to the height of specimens in Figure 11, and the results of fracture toughness are shown in Table 6. The GFRP bars reinforced UHPC beams produced a higher fracture toughness at the ultimate bearing capacity than HRB400 steel reinforced UHPC beams with the same reinforcement ratio. This was because the load of specimens was mainly determined by rebars when UHPC beams were damaged. The tensile strength of GFRP rebars was higher than that of HRB400 steel reinforcements with the same diameter, so GFRP rebars improved the flexural strength of UHPC beams. According to Eqs. (4) and (5), the high ultimate bearing capacity generated by the GFRP rebars also produced a high fracture toughness. The variation pattern of size effect on fracture toughness of GFRP

bars reinforced UHPC beams and HRB400 steel reinforced UHPC beams was consistent with that of equivalent bending stress. The size effect was shown for  $K_{IC}$  of GFRP bars reinforced UHPC beams with low reinforcement ratio, and the  $K_{IC}$  of GFRP bars reinforced UHPC beams with high reinforcement ratio had no size effect. However, no size effect was shown for  $K_{IC}$  of HRB400 steel reinforced UHPC beams. This was consistent with the findings from Zhang et al **Error! Reference source not found.** Compared to  $a/h$  (ratio of critical crack extension length to specimen height), the equivalent bending stress had a higher influence on the size effect of the  $K_{IC}$  of UHPC beams in this paper.

#### 4.4 Size effect on normalized deflection

The normalized deflection ( $\delta/L$ ) is defined as the ratio of the midspan deflection to the span length of the UHPC beams. The equivalent bending stress versus normalized deflection curves are provided in Figure 12. The size effect on normalized deflection at ultimate bearing capacity is provided in Figure 13. The deflection, normalized deflection and equivalent bending stress corresponding to the ultimate bearing capacity are summarized in Table 8.

The experimental results reflected the size effect on the normalized deflection: When the test beams reached the ultimate bearing capacity, the small GFRP bars reinforced UHPC beams produced higher normalized deflection capacities than large UHPC beams whereas the small HRB400 steel reinforced UHPC beams produced weaker normalized deflection capacities than large UHPC beams (Figure 13). However, the size had different effects on the equivalent bending stress and normalized deflection

of GFRP bars reinforced UHPC beams with high reinforcement ratio: the equivalent bending stress of large beam was higher than that of small beam whereas the normalized deflection of large beam was smaller than that of small beam (Figure 9 and Figure 13).

From a single force state, the normalized deflection of GFRP bars reinforced UHPC beams had size effect such as ultimate bearing capacity. However, it could be seen from the whole deflection process (Figure 12) that the deflection of GFRP bars reinforced UHPC beams had no size effect. No size effect was shown for normalized deflection of HRB400 steel reinforced UHPC beams from a single force state or ultimate bearing capacity.

#### **4.5 Size effect on ductility**

The ductility index of the UHPC beams at the ultimate bearing capacity is shown in Table 8, and the size effect on ductility is illustrated in Figure 14. The ductility index of GFRP bars reinforced UHPC beams (HRB400 steel reinforced UHPC beams) with 0.68% reinforcement ratio were 1.198 (1.201) and 1.222 (1.768) for small and large specimens, respectively, while those of GFRP bars reinforced UHPC beams (HRB400 steel reinforced UHPC beams) with 1.17% reinforcement ratio were 1.176 (1.198) and 1.181 (1.378) for small and large specimens. The ductility of GFRP bars reinforced UHPC beams was better when the beam size was large. This indicated that no size effect was shown for ductility of GFRP bars reinforced UHPC beams. The same was true for HRB400 steel reinforced UHPC beams. However, it is necessary to conduct more in-depth research of the size effect on the ductility of flexural UHPC beams with GFRP bars, since there are few studies on this issue.

## 5. Conclusions

This study investigates the size effect on the flexural performance of the GFRP rebars reinforced UHPC beams and HRB400 steel reinforced UHPC beams with two different reinforcement ratios. Two different sizes of UHPC beams were tested using four-point bending. From the above discussions, the following conclusions were demonstrated.

(1) The tensile failure was observed in GFRP rebars reinforced UHPC beams, balanced-reinforced failure was found for HRB400 steel rebars reinforced UHPC beams. The GFRP rebars reinforced UHPC beams changed from having a certain size effect to no size effect with the increase of reinforcement ratio. The HRB400 steel reinforced UHPC beams had no size effect, and this result was not affected by the reinforcement ratio.

(2) The maximum crack width, number of cracks and average crack spacing of UHPC beams was sensitive to specimen size that the maximum crack width, number of cracks and average crack spacing of UHPC beams with GFRP bars and HRB400 steel reinforcements increased significantly with the increase of specimen size.

(3) There was no size effect on the deflection of UHPC beams during the whole loading process. When the test beams reached the ultimate bearing capacity, the normalized deflection of GFRP bars reinforced UHPC beams increased with the decrease of specimen size, which had a certain size effect. The normalized deflection of HRB400 steel reinforced UHPC beams decreased with the decrease of specimen size, which had no size effect.

(4) No size effect was shown for ductility calculated by energy approach of GFRP bars reinforced UHPC beams and HRB400 steel reinforced UHPC beams.

## **Acknowledgments**

This research was supported by a research grant provided by the Natural Science Foundation of China (No. 51968013, 52022024) and Guang Xi Key Laboratory of New Energy and Building Energy Saving (No. 19-J-21-2, 22-J-21-14). Any opinions, findings and conclusions expressed in this paper do not necessarily reflect the view of the sponsors.

## **COMPETING INTERESTS**

The authors declare that they have no competing interests.

## **DATA AVAILABILITY**

Some or all data, models, or code that support the findings of this study are available from the corresponding author upon reasonable request.

## **References**

- [1] Weibull W. A statistical distribution function of wide applicability. *J Appl Mech* 1951, 18:293-7.
- [2] Bažant ZP. Size effect in blunt fracture: concrete, rock, metal. *J Eng Mech* 1984, 110:518-35.
- [3] Carpinteri A. Fractal nature of material microstructure and size effects on apparent mechanical properties. *Mech Mater*, 1994, 18(2):89-101.
- [4] Bažant ZP, Kim JK. Size effect in shear failure of longitudinally reinforced beam. *Aci J* 1984, 81(5):456-468.

- [5] Bažant ZP, Planas J. Fracture and Size Effect in Concrete and Other Quasibrittle Materials. Epfl 1997.
- [6] Wittmann FH, Mihashi H, Nomura N. Size effect on fracture energy of concrete. Eng Fract Mech 1990, 35(1-3):107-115.
- [7] Rossi P, Wu X, Maou FL, Belloc A. Scale effect on concrete in tension. Mater Struct 1994, 27(8):437-444.
- [8] Abdalla HM, Karihaloo BL. Determination of size-independent specific fracture energy of concrete from three-point bend and wedge splitting tests. Mag Concrete Res 2003, 55(2):133-141.
- [9] Lepech MD, Li VC. Preliminary findings on size effect in ECC structural members in flexure. In: Proceedings of the seventh international symposium on brittle matrix composites, Warsaw, Poland; 2003. p. 57–66.
- [10] Kim DJ, Naaman AE, El-Tawil S. Correlation between tensile and bending behavior of FRC composite with scale effect. In: Fracture mechanics of concrete and concrete structures – High performance, fiber reinforced concrete, special loadings and structural applications. Korea Concrete Institute; 2010. p. 1379– 85.
- [11] Alca N, Alexander SD, Macgregor JG. Effect of size on flexural behavior of high-strength concrete beams. Aci Struct J 1997, 94(1): 59-67.
- [12] Appa RG, Vijayanand I, Eligehausen R. Studies on ductility and evaluation of minimum flexural reinforcement in RC beams. Mater Struct 2008, 41 (4): 759-771.
- [13] Chen, X., Wan, D.-W., Jin, L.-Z., Qian, K., Fu, F., Experimental studies and microstructure analysis for ultra high-performance reactive powder concrete, Construction and Building Materials, 2019, 229, 116924

- [14] X Cao, XF Deng, LZ Jin, F Fu, K Qian, Shear capacity of reactive-powder-concrete beams using high-strength steel reinforcement, Proceedings of the Institution of Civil Engineers: Structures and Buildings
- [15] JSCE. Recommendations for design and construction of ultra-high strength fiber reinforced concrete structures (Draft). Tokyo, Japan: Japan Society of Civil Engineers; 2006.
- [16] Mahmud GH, Yang Z, Hassan A. Experimental and numerical studies of size effects of Ultra High Performance Steel Fibre Reinforced Concrete (UHPRFC) beams. Constr Build Mater 2013, 48(nov.):1027-1034.
- [17] Wille K, Parra-Montesinos GJ. Effect of Beam Size, Casting Method, and Support Conditions on Flexural Behavior of Ultra-High-Performance Fiber-Reinforced Concrete. Aci Mater J 2012, 109(3): p.379-388.
- [18] Nguyen DL, Kim DJ, Ryu GS, Koh KT. Size effect on flexural behavior of ultra-high-performance hybrid fiber-reinforced concrete. Compos Part B 2013, 45(1):1104-1116.
- [19] Yoo DY, Banthia N, Kang ST, Yoon YS. Size effect in ultra-high-performance concrete beams. Eng Fract Mech 2016:86-106.
- [20] Reineck KH, Frettlor B. Tests on scale effect of UHPRFC under combined bending and axial forces. In: The 3rd fib international congress, Washington DC; 2010. p.14 [paper 54].
- [21] Chandransu K, Naaman AE. Comparison of tensile and bending response of three high performance fiber-reinforced cement composites. In: Naaman AE, Reinhardt HW, editors. Proceedings of the fourth international workshop on high performance fiber reinforced cement, composites (HPRCC4), Ann Arbor, MI, USA; 2003. p. 259–74.

- [22] Yoo DY, Zi G, Kang ST, Yoon YS. Biaxial flexural behavior of ultra-high-performance fiber-reinforced concrete with different fiber lengths and placement methods. *Cement Concrete Comp* 2015, 63:51-66.
- [23] Ferrara L. High performance fiber reinforced self-compacting concrete (HPFR-SCC): a “smart material” for high end engineering applications. In: *Third international workshop on heterogeneous architectures and computing*, Madrid; 2012. p. 325–34.
- [24] Yang IH, Joh C, Kim BS. Structural behavior of ultra high performance concrete beams subjected to bending. *Eng Struct* 2010, 32(11):3478-3487.
- [25] Yoo DY, Kang ST, Yoon YS. Erratum: Effect of fiber length and placement method on flexural behavior, tension-softening curve, and fiber distribution characteristics of UHPFRC. *Constr Build Mater* 2014, 64:67-81.
- [26] Wang, L., Shen, N., Zhang, M., Fu, F., Qian, K. Bond performance of Steel-CFRP bar reinforced coral concrete beams, *Construction and Building Materials*, 2020, 245, 118456
- [27] Wang, L., Song, Z., Yi, J., ...Fu, F., Qian, K. Experimental Studies on Bond Performance of BFRP Bars Reinforced Coral Aggregate Concrete, *International Journal of Concrete Structures and Materials*, 2019, 13(1), 52
- [28] Zhang XF, Xu SL. A comparative study on five approaches to evaluate double- K fracture toughness parameters of concrete and size effect analysis. *Eng Fract Mech* 2011, 78(10):2115-2138.
- [29] Gao, S., Guo, L., Fu, F., Zhang, S. Capacity of semi-rigid composite joints in accommodating column loss, *Journal of Constructional Steel Research*, 2017, 139, pp. 288–301
- [30] Fu, F., Parke, G.A.R. Assessment of the Progressive Collapse Resistance of Double-Layer Grid

Space Structures Using Implicit and Explicit Methods, *International Journal of Steel Structures*, 2018, 18(3), pp. 831–842

[31] Fu, F., Lam, D., Ye, J., Moment resistance and rotation capacity of semi-rigid composite connections with precast hollowcore slabs, *Journal of Constructional Steel Research*, 2010, 66(3), pp. 452–461

[32] [1] Fu, F., Lam, D., Ye, J., Modelling semi-rigid composite joints with precast hollowcore slabs in hogging moment region, *Journal of Constructional Steel Research*, 2008, 64(12), pp. 1408–1419

[33] Qian, K., Lan, X., Li, Z., Li, Y., Fu, F. Progressive collapse resistance of two-storey seismic configured steel sub-frames using welded connections, *Journal of Constructional Steel Research*, 2020, 170, 106117

[34] Yoo DY, Yoon YS. Structural performance of ultra-high-performance concrete beams with different steel fibers. *Eng Struct* 2015, 102(NOV.1):409-423.

[35] Naaman AE, Jeong SM. Structural ductility of concrete beams prestressed with FRP tendons. In: *Proceedings of the second international RILEM symposium (FRPRCS-2): non-metallic (FRP) for concrete structures*, Ghent, Belgium;1995. p. 379-86.

[36] Jo BW. Ductility Evaluation of Prestressed Concrete Beams with CFRP Tendons. *J Reinf Plast Comp* 2004, 23(8):843-859.

[37] Abdelkarim OI, Ahmed EA, Mohamed HM, et al. Flexural strength and serviceability evaluation of concrete beams reinforced with deformed GFRP bars. *Eng Struct* 2019, 186:282-296.

[38] Park SH, Dong JK, Ryu GS, Koh KT. Tensile behavior of Ultra High Performance Hybrid Fiber Reinforced Concrete. *Cement Concrete Comp* 2012, 34(2):172-184.

[39] Li VC, Maalej M. Toughening in Cement Based Composites. Part II: Fiber Reinforced Cementitious Composites. *Cement Concrete Comp* 1996, 18(4):239-249.

[40] Zhang XF, Xu SL. A comparative study on five approaches to evaluate double- K fracture toughness parameters of concrete and size effect analysis. *Eng Fract Mech* 2011, 78(10):2115-2138.

## **Figure captions**

Figure 1. Details of test program; (a) details of small test beams (G/S-0.68/1.17-250), (b) details of large test beams (G/S-0.68/1.17-500), (c) section details of test beams.

Figure 2. Details of test setup.

Figure 3. Distribution of moment, shear, and cracks along beam.

Figure 4. Photo of specimen with multiple cracks.

Figure 5. Crack patterns and failure modes; (a) cracking behavior and failure modes of UHPC beams, (b) the tensile failure of GFRP bars reinforced UHPC beams, (c) the balanced-reinforced failure of HRB400 steel reinforced UHPC beams.

Figure 6. The load and mid-span deflection curves of UHPC beams.

Figure 7. The load and strain curves in rebar of UHPC beams.

Figure 8. The schematic diagram of the load–deflection curve of beams with FRP bars and steel bars showing the calculated energies; (a) FRP bars reinforced beams [35], (b) steel reinforced beams [36].

Figure 9. Size effects on the equivalent bending stress of the UHPC beams.

Figure 10. Size effect on cracking behavior of the UHPC beams; (a) Max. crack width,

(b) number of cracks within zone 1, (c) average crack spacing.

Figure 11. Size effect on fracture toughness parameter.

Figure 12. The equivalent bending stress versus normalized deflection curve of UHPC beams for different size.

Figure 13. Size effect on normalized deflection at ultimate strength.

Figure 14. Size effect on ductility of the UHPC beams at ultimate bearing capacity.

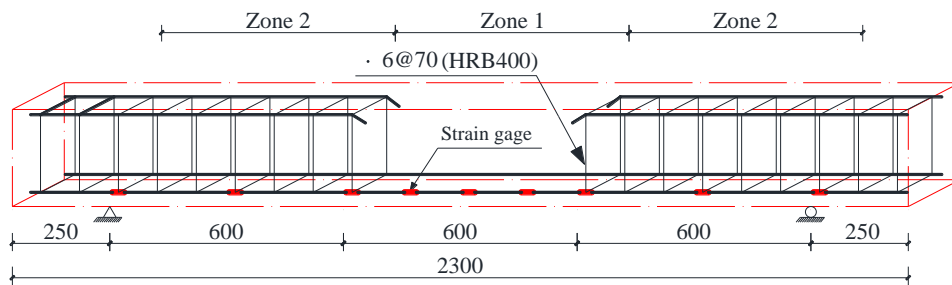


Figure 1(a)

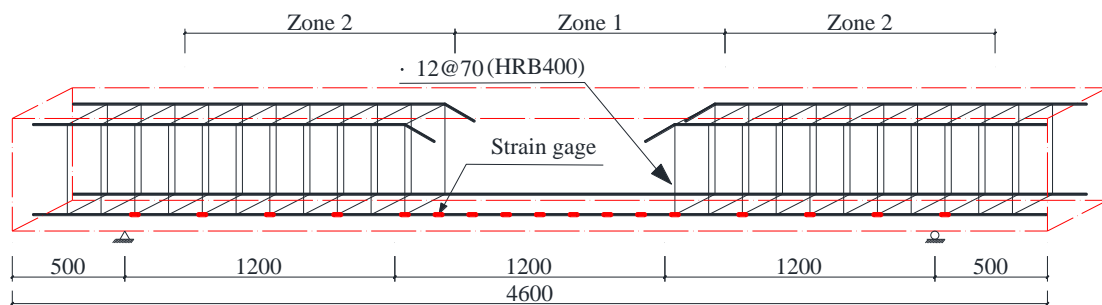
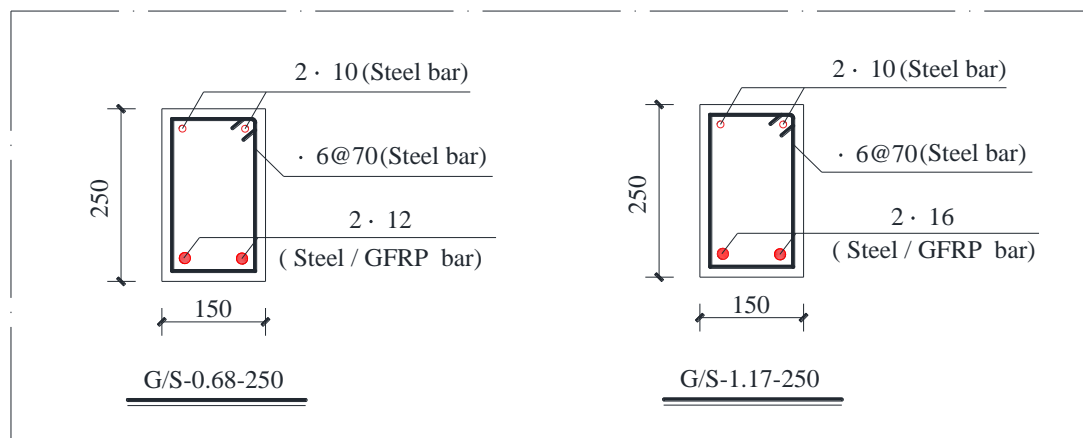


Figure 1(b)



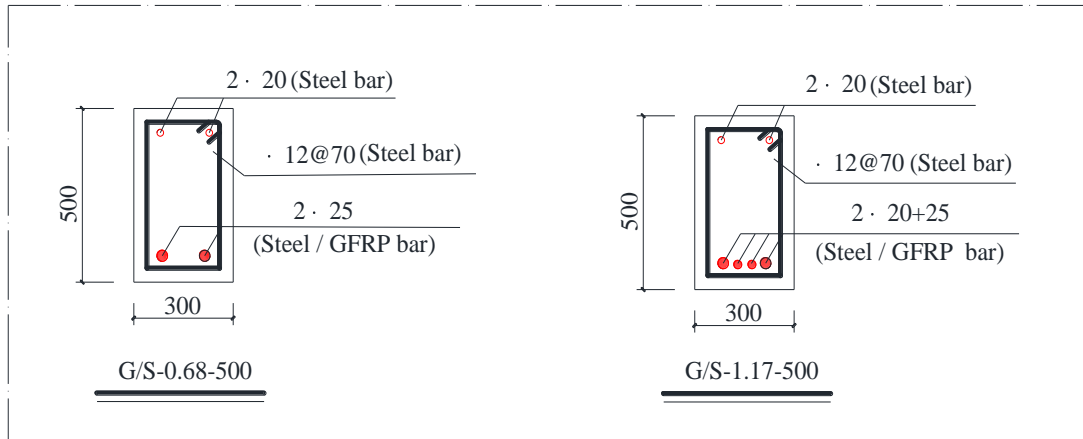


Figure 1(c)

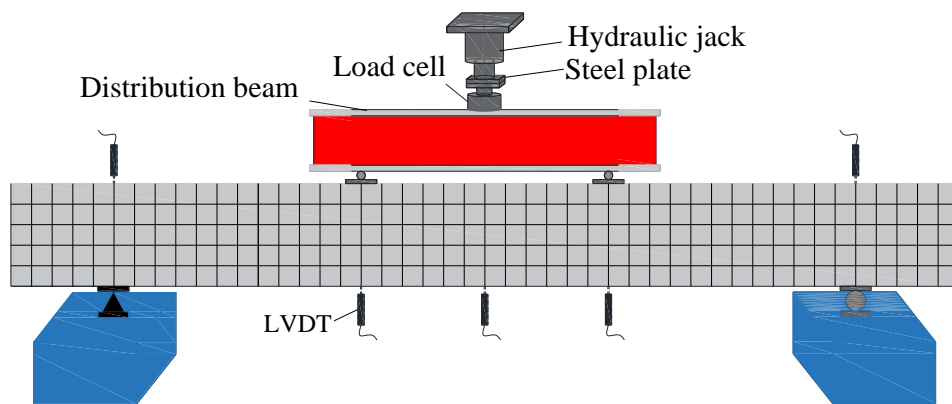


Figure 2

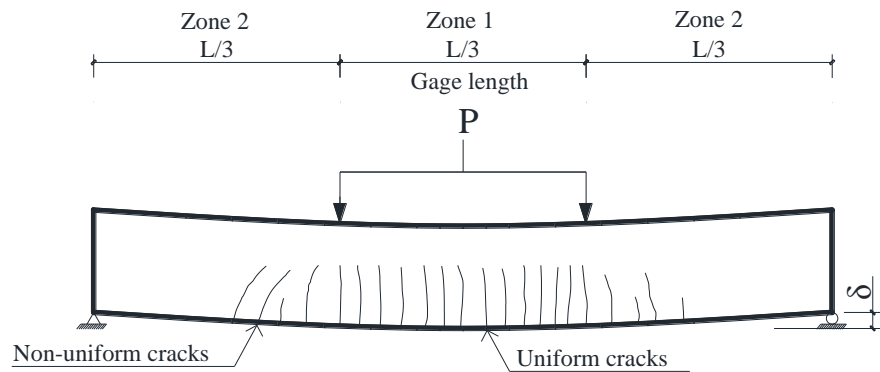


Diagram M due to P

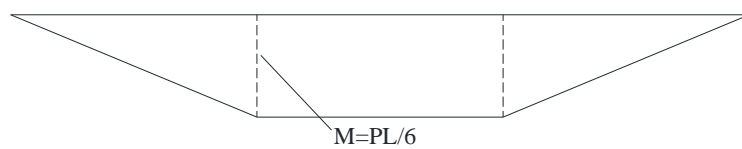


Diagram V due to P

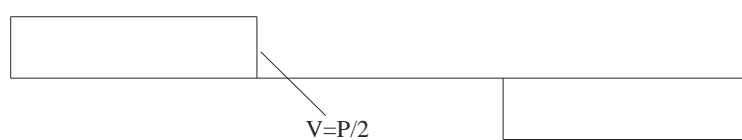


Figure 3

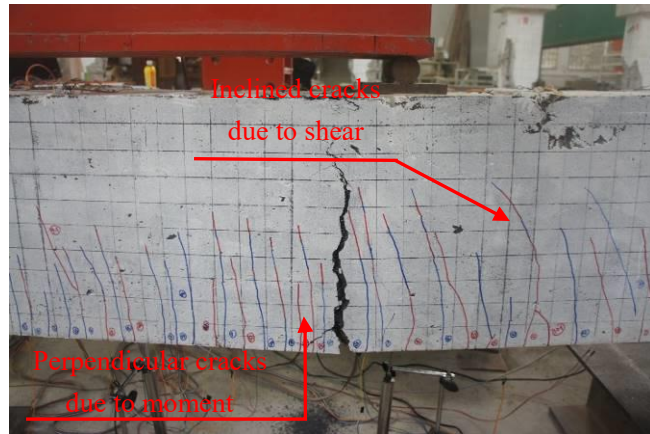


Figure 4





Figure 5(a)

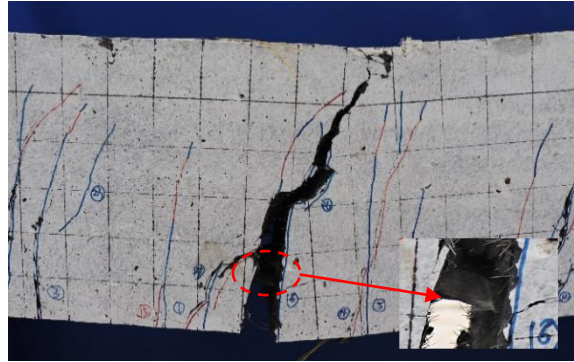


Figure 5(b)

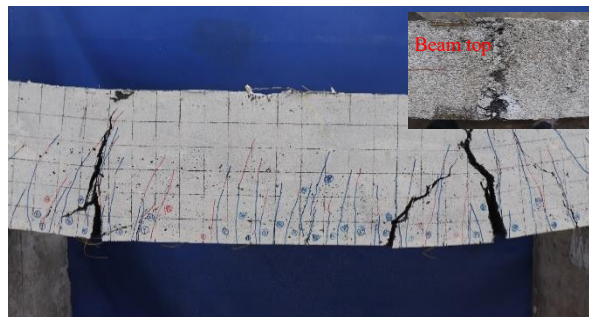


Figure 5(c)

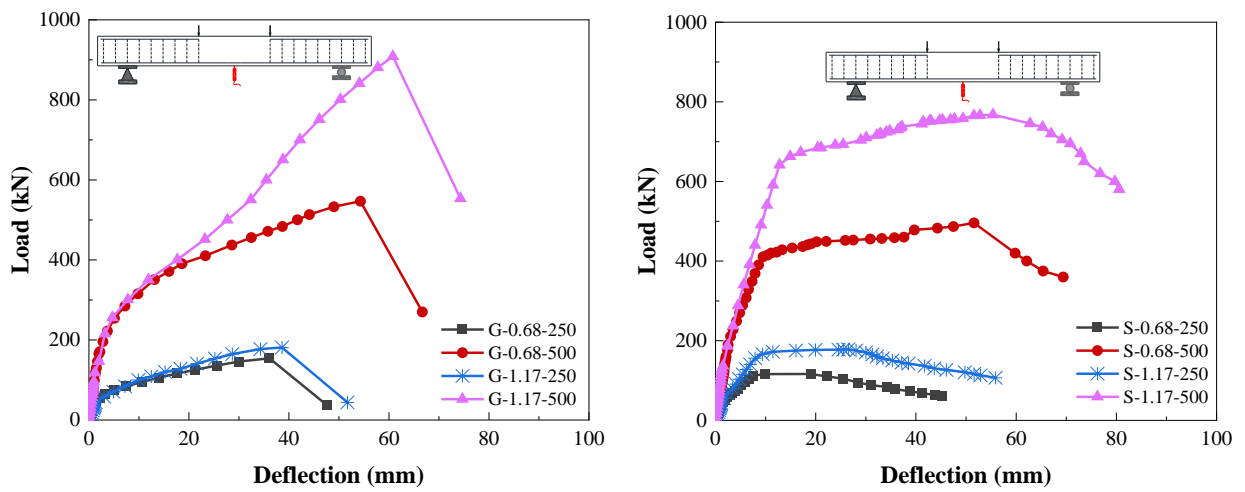


Figure 6

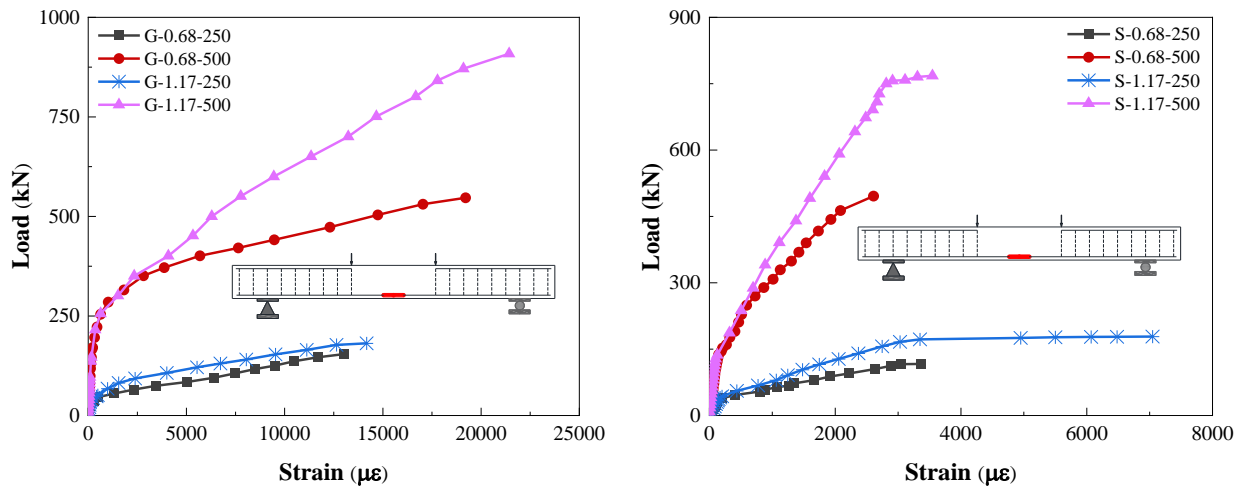


Figure 7

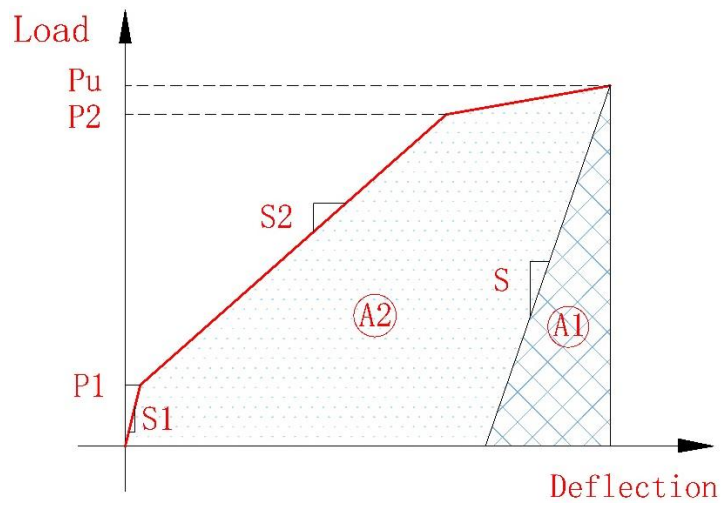


Figure 8(a)

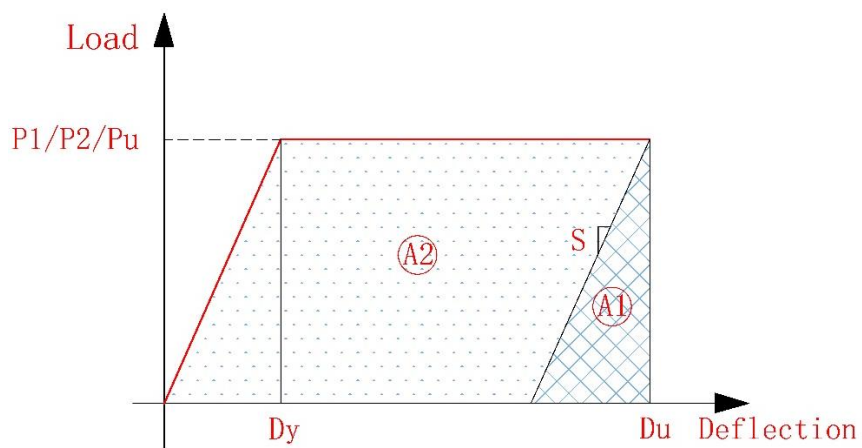


Figure 8(b)

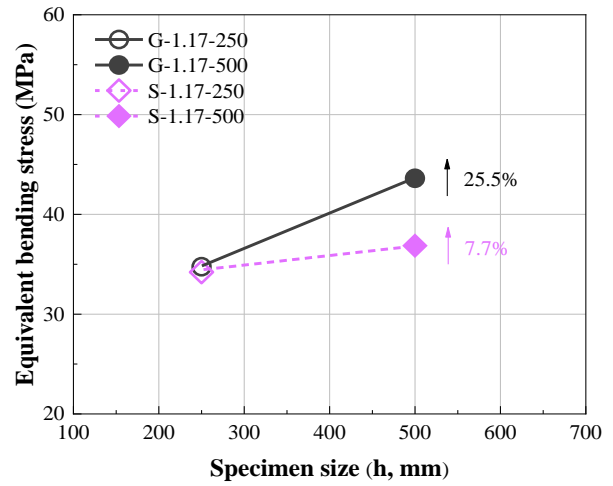
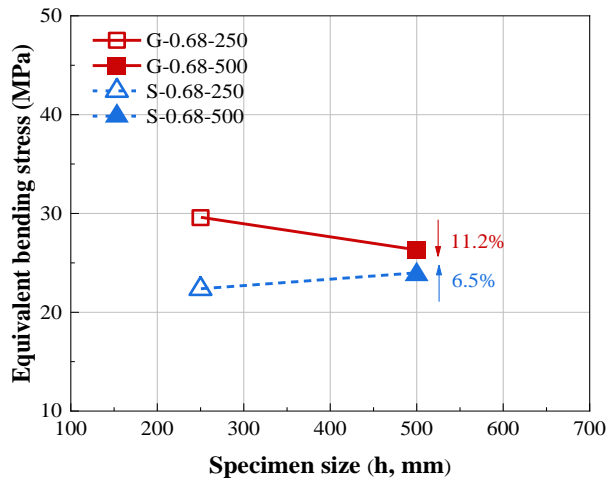


Figure 9

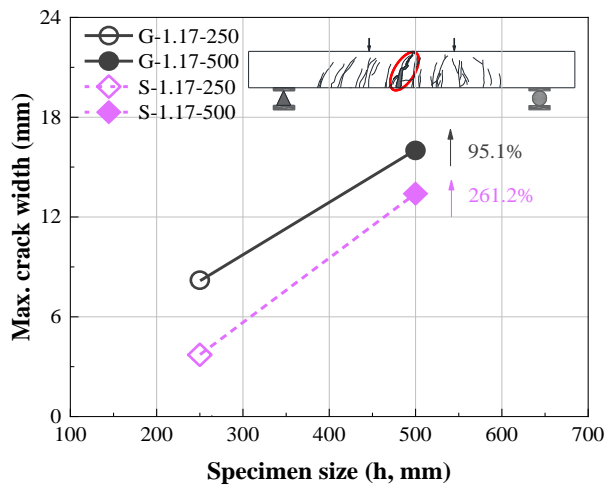
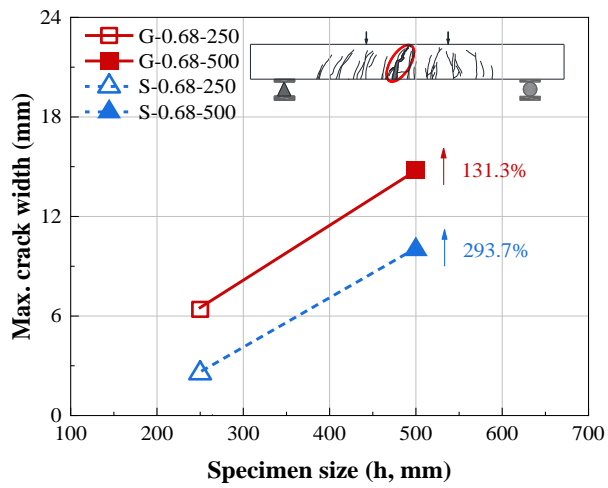


Figure 10(a)

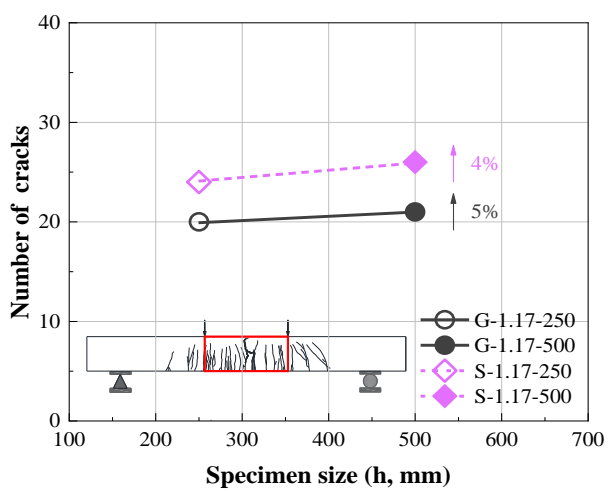
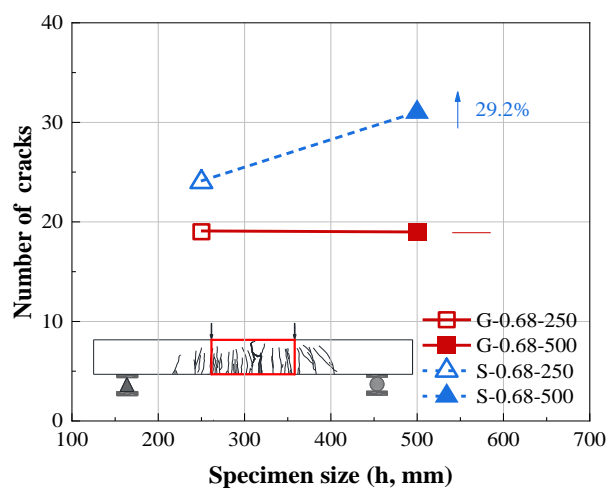


Figure 10(b)

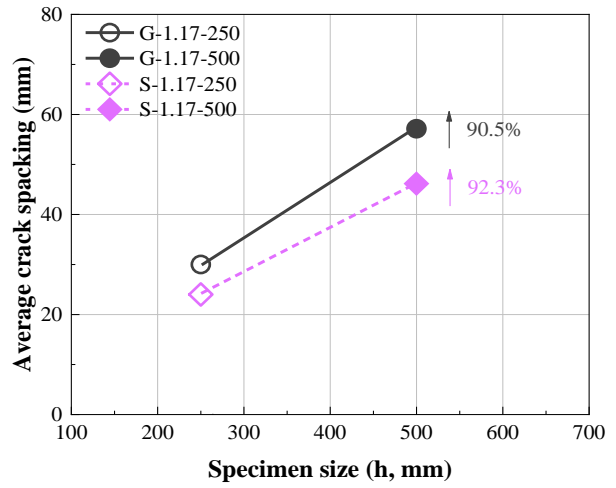
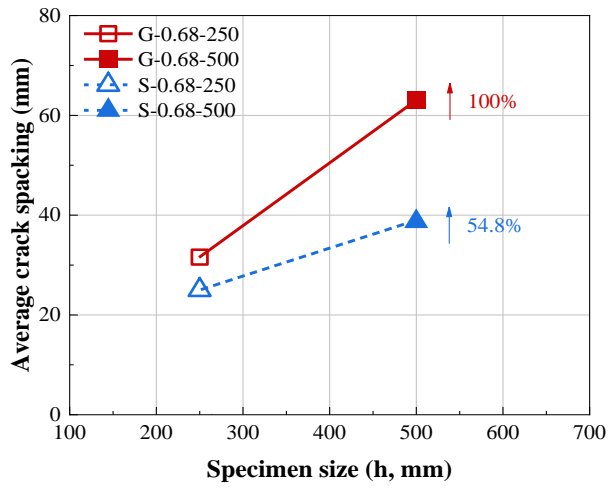


Figure 10(c)

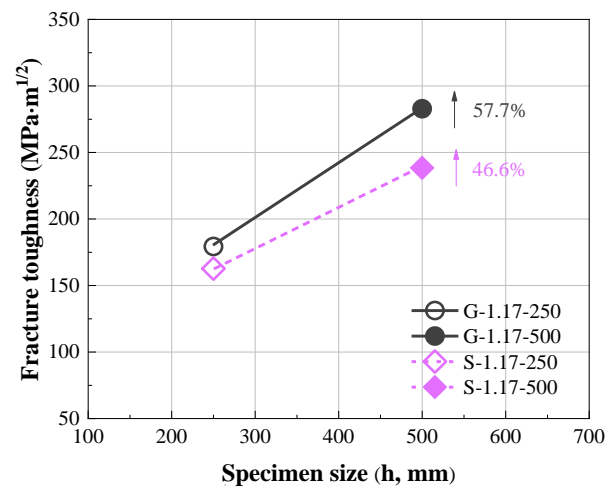
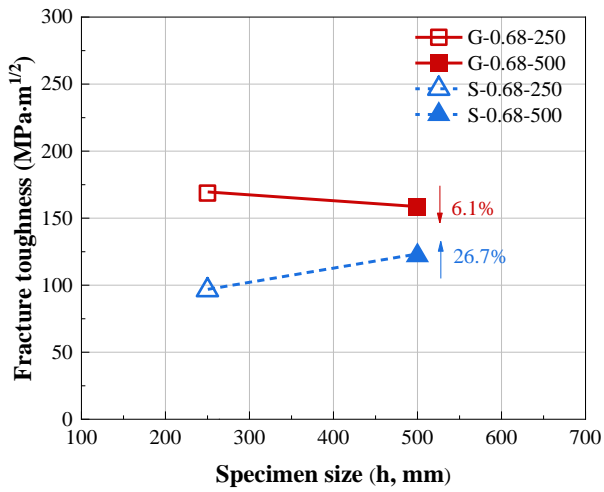


Figure 11

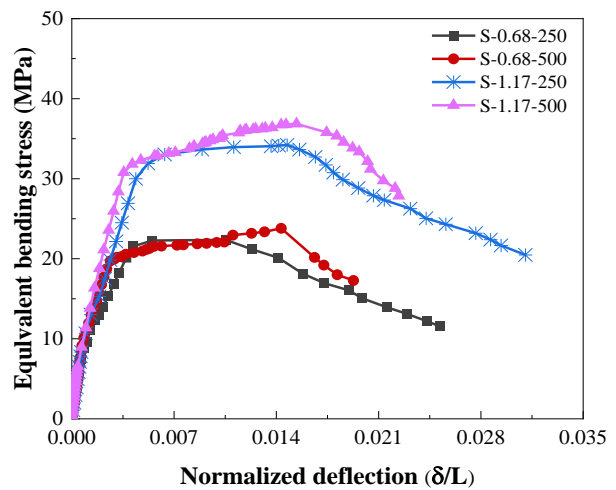
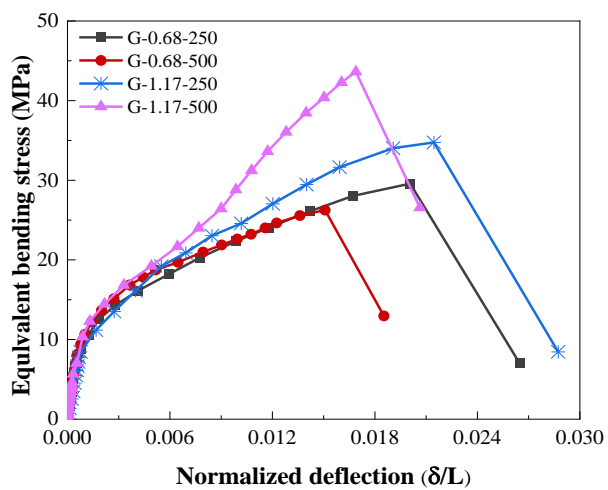


Figure 12

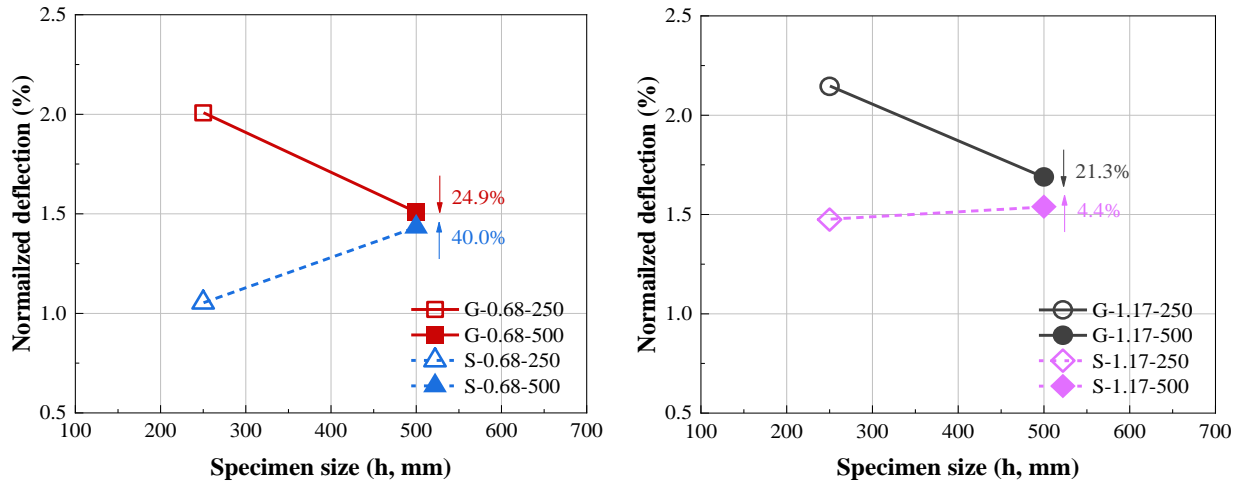


Figure 13

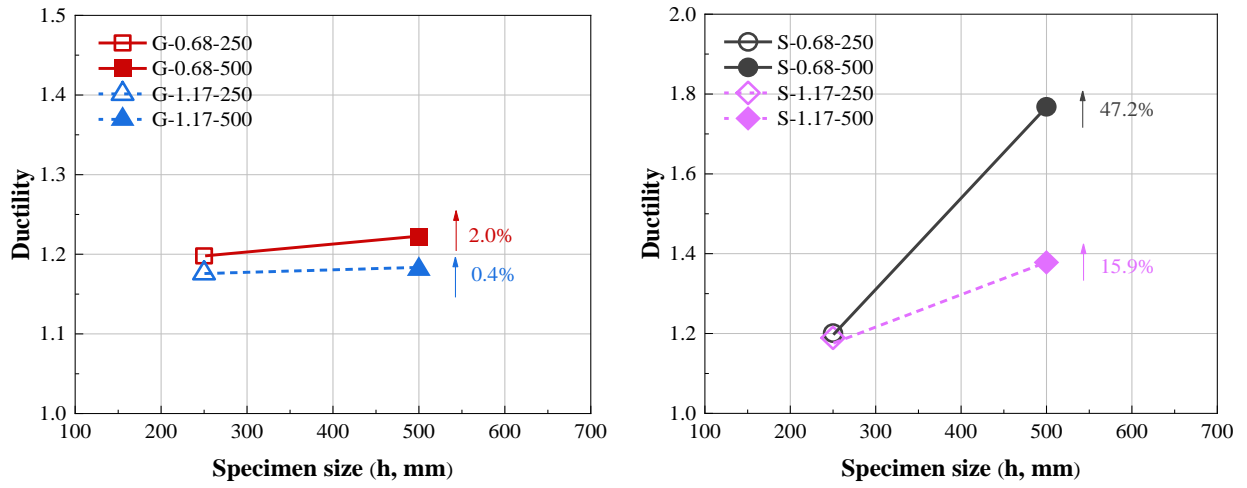


Figure 14

Table 1. Mix design of UHPC

Cement	Silica sand			Silica fume	Super-plasticizer	Water	Steel fibers
	Coarse	Medium	Fine				
1.00	0.20	0.80	0.20	0.30	0.02	0.23	2%

Where: Steel fiber is the volume dose.

Table 2. Mechanical properties of UHPC

$E_c$ (GPa)	$f_{cu}$ (MPa)	$f_c$ (MPa)	$f'_c$ (MPa)	$f_t$ (MPa)
45.6	139.7	114.5	102.2	6.4

Where  $E_c$  = elastic modulus of UHPC,  $f_{cu}$  = cubic compressive strength of UHPC,  $f_c$  = prismatic compressive strength of UHPC,  $f'_c$  = cylindrical compressive strength of UHPC,  $f_t$  = tensile strength of UHPC.

Table 3. Properties of steel fibers

$d_f$ (mm)	$L_f$ (mm)	Aspect ratio ( $L_f / d_f$ )	Density (g/cm <sup>3</sup> )	$f_t$ (MPa)	$E_f$ (GPa)
0.22	13	59.1	7.8	2000	200

Where  $d_f$  = diameter of fiber,  $L_f$  = length of fiber,  $f_t$  = tensile strength of fiber, and  $E_f$  = elastic modulus of fiber.

Table 4. Main parameters of UHPC beams

Specimen	Section form	$l$ /mm	$L$ /mm	$b \times h$ /mm <sup>2</sup>	Rebar type	Tensile rebar	$\rho$ /%	Bent shear stirrup
G-0.68-250	rectangle	2300	1800	150×250	GFRP	2C12	0.68	C6@70
G-0.68-500	rectangle	4600	3600	300×500	GFRP	2C25	0.68	C12@70
G-1.17-250	rectangle	2300	1800	150×250	GFRP	2C16	1.17	C6@70
G-1.17-500	rectangle	4600	3600	300×500	GFRP	2C20+2C25	1.17	C12@70
S-0.68-250	rectangle	2300	1800	150×250	HRB400	2C12	0.68	C6@70
S-0.68-500	rectangle	4600	3600	300×500	HRB400	2C25	0.68	C12@70
S-1.17-250	rectangle	2300	1800	150×250	HRB400	2C16	1.17	C6@70
S-1.17-500	rectangle	4600	3600	300×500	HRB400	2C20+2C25	1.17	C12@70

Where  $l$  = length of beam,  $L$  = span length of beam,  $b$  = width of beam,  $h$  = height of beam and  $\rho$  = ratio of longitudinal reinforcement.

Table 5. Properties of steel and GFRP bars

Types	$d(\text{mm})$	$A(\text{mm}^2)$	$E(\text{GPa})$	$f_y(\text{MPa})$	$f_u(\text{MPa})$
GFRP rebar	12	113.09	44.2	—	927.7
	16	201.06	46.0	—	606.8
	20	314.16	46.2	—	595.3
	25	480.87	43.5	—	778.2
HRB400 steel rebar	12	113.09	200	452.3	603.4
	16	201.06	200	441.7	598.1
	20	314.16	200	429.7	602.3
	25	490.87	200	406.4	598.2

Where  $d$  = diameter of rebar,  $A$  = area of rebar,  $E$  = elastic modulus of rebar,  $f_y$  = yield strength of steel rebar, and  $f_u$  = ultimate strength of rebar.

Table 6. Summary of experimental results for UHPC beams with GFRP rebars and HRB400 steel reinforcements.

Specimen	$P_u(\text{kN})$	$M_u(\text{kN}\cdot\text{m})$	$\sigma_{f,u}$	$a(\text{mm})$	$K_{IC}(\text{MPa}\cdot\text{m}^{1/2})$	Failure mode
G-0.68-250	154.0	46.20	29.57	237.5	168.46	Tensile failure
G-0.68-500	546.8	328.08	26.25	441.7	158.13	Tensile failure
G-1.17-250	181.0	54.30	34.75	231.8	179.31	Tensile failure
G-1.17-500	908.6	545.16	43.61	450.1	282.83	Tensile failure
S-0.68-250	116.4	34.92	22.35	221.5	96.30	Balanced-reinforced failure
S-0.68-500	495.8	297.48	23.80	423.3	122.00	Balanced-reinforced failure

S-1.17-250	178.2	53.46	34.21	227.1	162.62	Balanced-reinforced failure
S-1.17-500	767.8	460.68	36.85	449.8	238.37	Balanced-reinforced failure

Where  $P_u$  = the peak load,  $M_u$  = the ultimate moment,  $\sigma_{f,u}$  = the equivalent bending stress for ultimate moment,

$\mu_e$  = ductility index,  $a$  = critical crack extension length,  $K_{IC}$  = the fracture toughness.

Table 7. The number of cracks, average crack spacing and max. crack width of the UHPC beams

Specimen	Cracks within zone 1				Cracks within zones 1 and 2 Number of cracks	Zone 1 cracks as percentage of total <sup>a</sup> (%)
	Number of cracks	Length of zone 1 (mm)	Crack spacing (mm)	Max. crack width (mm)		
G-0.68-250	19	600	31.58	6.4	29	65.5
G-0.68-500	19	1200	63.16	14.8	30	63.3
G-1.17-250	20	600	30.00	8.2	34	58.8
G-1.17-500	21	1200	57.14	16	36	58.3
S-0.68-250	24	600	25.00	2.54	38	63.2
S-0.68-500	31	1200	38.71	10	43	72.1
S-1.17-250	25	600	24.00	3.71	39	64.1
S-1.17-500	26	1200	46.15	13.4	46	56.5

where <sup>a</sup> Calculated by taking the average number of cracks in zone 1 and dividing by the average of the total number of cracks in zone 1 and 2.

Table 8. Calculation results of equivalent bending stress, normalized deflection, and ductility at

ultimate bearing capacity.

Specimen	$\delta$ (mm)	$\delta / L$ (%)	$\sigma_{fl}$ (MPa)	$\mu$
G-0.68-250	36.126	2.007	29.57	1.198
G-0.68-500	54.300	1.508	26.25	1.222
G-1.17-250	38.617	2.145	34.75	1.176
G-1.17-500	60.800	1.689	43.61	1.181
S-0.68-250	18.977	1.054	22.35	1.201
S-0.68-500	51.600	1.433	23.80	1.768
S-1.17-250	26.524	1.474	34.21	1.189
S-1.17-500	55.400	1.539	36.85	1.378

Where  $\delta$  = the deflection,  $\delta / L$  = the normalized deflection,  $\sigma_{fl}$  = the equivalent bending stress, and  $\mu$  = the ductility at ultimate bearing capacity.